Journal of Fundamental and Applied Sciences

Research Article

ISSN 1112-9867

Available online at http://www.jfas.info

MAGNETIC ADSORBENT BASED ON CARBOXYMETHYL CELLULOSE FOR METHYLENE BLUE UPTAKE FROM AQUEOUS MEDIA

Tayeb Benhalima[1, 2], Amina Sadi[1], Hafida Ferfera-Harrar[1]

[1]Department of Macromolecular Chemistry, Faculty of Chemistry, University of Sciences and Technology Houari Boumediene (USTHB) Algiers, Algeria

[2]Unité de Recherche en Analyse et Développement Technologique en Environnement (UR-ADTE). Centre de recherche scientifique et technique en analyses physico-chimiques, BP 384, Bou-Ismail CP 42004, Tipaza, Algeria

Received: 29 September 2023 / Accepted: 10 December 2023 / Published: 11 December 2023

ABSTRACT

Cross-linked carboxymethyl cellulose/Dextran sulfate (CMC/DS) magnetic nanocomposite beads, incorporating oxide iron nanoparticles (Fe3O4) via ionotropic gelation, were synthesized and characterized using FTIR, SEM/EDX, NanoSEM, XRD, TGA, and VSM. The addition of Fe3O4 imparted a porous structure, enhanced thermal stability, and superparamagnetic properties, facilitating efficient separation through an external magnetic field. Evaluated for methylene blue (MB) adsorption, the nanocomposites exhibited favorable pseudo-second-order kinetics, driven by chemisorption via electrostatic interactions. The Langmuir model described the adsorption isotherms, with a slightly reduced maximum equilibrium capacity (331 mg g-1) compared to the matrix (384 mg g-1). Demonstrating excellent reusability over five cycles, these magnetic nanocomposites present promising prospects for environmental remediation.

Keywords: Carboxymethyl cellulose; Hydrogels; Magnetic nanoparticles; Adsorption; Reuse

Author Correspondence, e-mail: harrarhafida@yahoo.fr

doi: http://dx.doi.org/10.4314/jfas.1345

1. INTRODUCTION

In recent years, climate change, the growth of the human population and the insufficiency of water resources have made the remediation of polluted water an urgent necessity [1]. Among the organic or inorganic pollutants, dyes are considered to be the most dangerous even if they are most often present in trace amounts, due to their highly toxic and carcinogenic character and their non-degradable and persistent nature [2]. In front of this critical situation, many water treatment methods are used for the dyes removal from wastewater. They include physical, chemical and biological processes. Among these processes, adsorption is considered to be one of the best alternative and economically attractive methods for wastewater treatment due to its convenience, ease of use, the simplicity of its design and its effectiveness. Various types of absorbent have been developed for the removal of dyes present in water such as clays, activated carbon, natural and synthetic polymers [3].

Adsorbents separating from the purified medium is one of a major problem in water treatment technology. Tedious filtration and centrifugation steps using energy-intensive pumping are often required to speed up the passage of liquid through filters. One of the ways being studied to develop magnetic adsorbents from hydrogel beads is to encapsulate magnetic nanoparticles within networks [4]. the desired magnetic properties of these hydrogel beads give them the advantage of being magnetically separated from the effluent to be treated.

The current work presents two environmental aspects in response to ecological concerns: on the one hand, it is part of a trend towards non-food valorization of agro-polymers, which are low cost and available, to develop materials such as polysaccharides-based hydrogels. On the other hand, the implementation of these materials as bioadsorbents in the treatment of polluted water. So, the aim of this study was to develop adsorbents materials that could be integrated into an industrial scale water treatment sector. In a first step, we synthesized magnetic iron oxide nanoparticles by the coprecipitation method that served, subsequently, to prepare magnetic hydrogel nanocomposite based on cross-linked carboxymethyl cellulose (CMC)/Dextran sulfate (DS) matrix network. The influence of Fe_3O_4 nanoparticles on the physic-chemical proprieties were of the developed magnetic beads investigated. Their aptitude for the adsorption of MB dye as a cationic pollutant model was tested under several

studied adsorption-controlling factors.

2. EXPERIMENTAL

2.1. Materials and procedures

Sodium carboxymethyl cellulose (CMC) 2500–6000 cps, sodium dextran sulfate (DS) Mw 7–20 kDa, were purchased from Sigma Aldrich. NaCl, $Al(NO_3)_3.9H_20$, sodium ndodecyl sulfate (SDS) and methylene blue (MB) were purchased from Sigma–Aldrich. $FeCl_3.6H_2O$, $FeSO_4.7H_2O$ were obtained from MERCK. Other chemicals were of analytical grades and were used as received.

2.2. Magnetic beads preparation

The synthesis of magnetic nanocomposite beads is given below. Aqueous mixture was prepared by dissolving required amount of CMC, DS and 0.2% of SDS surfactant in NaCl solution under vigorous stirring. After that, appropriate amounts of Fe_3O_4 magnetic nanoparticles initially synthesized was added to the previous mixture and keep under mechanical stirring for 1 h. The viscous mixture was extruded in the form of droplets into aqueous solution of $Al(NO_3)_3.9H_2O$ and the obtained beads were left overnight. Then, beads were collected by an external magnet, washed with double distilled water, and finally dried in oven at 60 °C.

2.3. Characeritaion

For dye adsorption measurements, the change in concentration was monitored periodically using a UV-visible spectrophotometer model Shimadzu UV-1650. A calibration curve was prepared by recording the absorbance values for MB solutions of known concentrations at λ max 664 nm. FTIR spectra with Attenuated Total Reflectance mode (ATR-FTIR) were performed on a spectrophotometer Bruker Vector 22 Spectrometer GmbH, in range of 4000–700 cm^{-1} , scans average of 128 and resolution of 4 cm^{-1} . The surface morphology of the beads was observed with environmental Quanta 250 Scanning Electron Microscope (SEM). For the microstructural and chemical characterization of beads, energy dispersive X-ray (EDX) analyses were recorded on the coupled SEM-EDX instrument.

2.4. Adsorption studies

Batch adsorption experiments were carried out at room temperature. Typically, 25 mg of hydrogel beads were dispersed in 25 mL of dye solution and stirred at 200 rpm on an orbital shaker. After adsorption, the magnetic beads were collected using a magnet and the remaining concentration of MB was evaluated using a UV spectrophotometer at 664 nm.

The adsorption capacity and the removal efficiency R (%) were calculated using the following **Eqs. (1)** and **(2)**, respectively:

$$q_t = \frac{C_0 - C_t}{m} \times V \qquad (1)$$

$$R(\%) = \frac{C_0 - C_t}{C_0} \times 100 \qquad (2)$$

Where q_t is the adsorption capacity at time t, m is the weight of the adsorbent (g) and V is the volume of the solution (L).

3. RESULTS AND DISCUSSION

3.1. Structural and physical properties

Magnetic nanocomposite and free-matrix hydrogels were formed instantaneously upon contact with the Al^{3+} cross-linking agent solution. the nanocomposite beads show a similar texture to that of free-matrix M0-C/D0.5, with millimetic sizes.

The SEM micrographs of MN nanoparticles, magnetic beads and the virgin matrix are grouped in Fig. 1. As shown from Fig. 1b, the nanoparticles are spherical with equivalent dimensions and a rough surface structure.

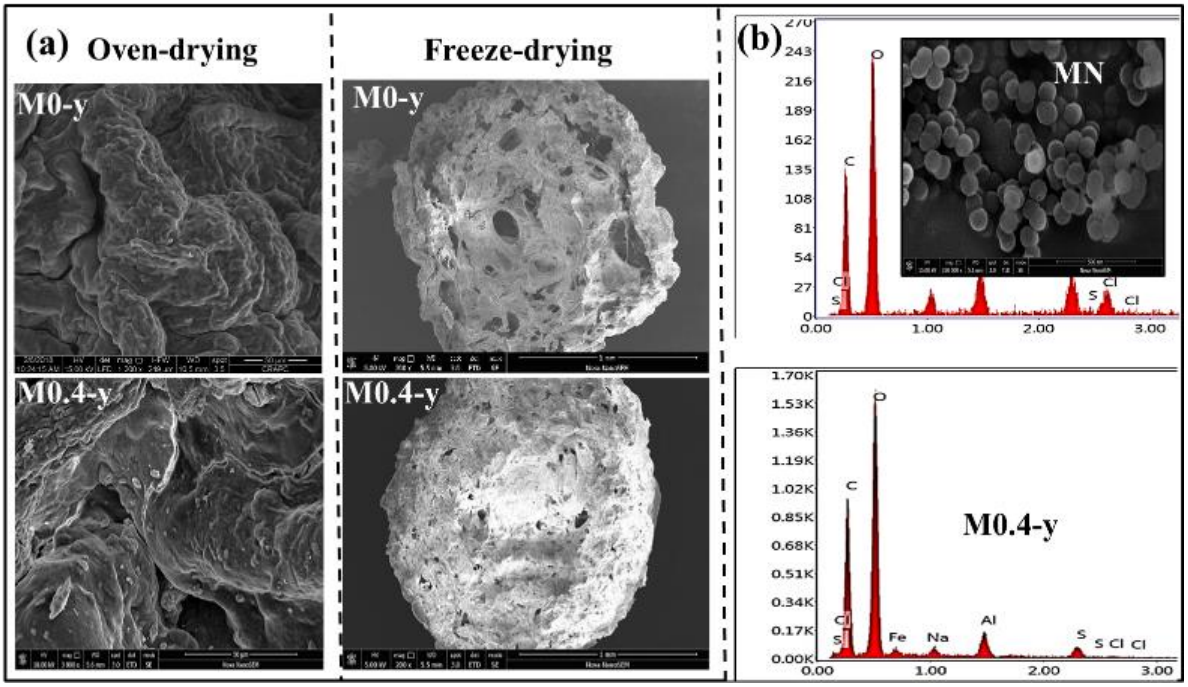

Fig.1. (a) SEM micrographs of the beads and Fe_3O_4nanoparticles as insert (b) EDX patterns

By analyzing the SEM micrographs of the beads presented in Fig. 1a, it is evident that the surface morphology of the nanocomposite beads differs from that of the matrix. The beads, after drying in the oven, exhibit relatively rough and compact external surfaces. Conversely, the surfaces of cross-sections taken after freeze drying reveal cavities and interstices, forming an interconnected microporous structure. This porous structure is likely conducive to enhancing their specific surface area, thereby improving their adsorption capacity for dyes [5]. Furthermore, the presence of Fe_3O_4 within the magnetic beads was confirmed by the EDX spectra (Fig. 1b), which displayed characteristic peaks for iron and oxygen elements, providing evidence of successful encapsulation.

Fig. 2 displays the XRD patterns of magnetic nanoparticles and the nanocomposite beads.

As observed, the diffractogrms of the prepared Fe_3O_4 nanoparticles present diffraction peaks of polycrystalline magnetite (PCPDFWIN v.2.02, PDF n ° 85-1436) at approximately 2θ of 30.3°, 35.5°, 37.27, 43.2°, 53.5°, 57° and 62.7° with Miller indices of (220), (311), (222), (400), (422), (511) and (440), respectively. The XRD pattern of the matrix indicates the amorphous nature of both polysaccharides (CMC and DS) as it shows no diffraction peaks. In contrast, the nanocomposites diffractogram reveals the characteristic peaks of Fe_3O_4

nanoparticles, suggesting that their crystal structure remained unchanged after being encapsulated within the beads

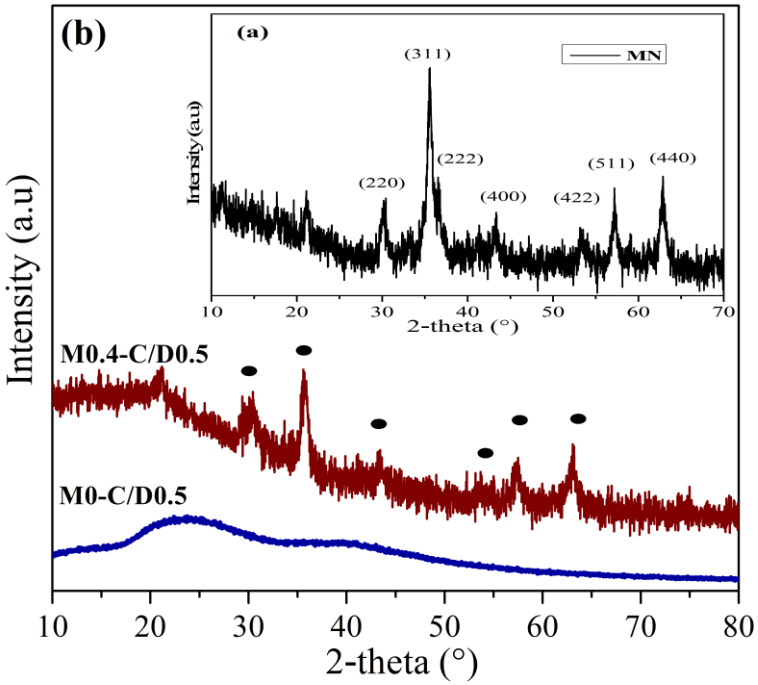

Fig.2. XRD patterns of magnetic nanoparticles, free hydrogel and its nanocomposites

Fig. 3 regroups FTIR spectra of Fe_3O_4 nanoparticles, CMC/DS matrix and its nanocomposite. The spectrum of the unloaded hydrogel M0-C/D0.5 primarily exhibits bands at 3465 cm^{-1} attributed to νO-H, at 1644 and 1435 cm^{-1} corresponding to the asymmetric and symmetric vibrations of of νC=O in COO- groups, respectively. Additionally, bands at 1260 and 830 cm^{-1} are ascribed to the asymmetric νS=O of ester sulfate and symmetric νCO-S of C-O-SO_3– groups [6]. The formation of the hydrogel is evident from the shift of the νC=O band and the appearance of an additional band at 1730 cm^{-1} due to the occurrence of electrostatic interactions between the COO^- groups and Al^{3+} ions of crosslinker [1,2,7].

Furthermore, the incorporation of magnetic nanoparticles in the beads induces shifts of some characteristic bands of the crosslinked matrix CMC/DS [8]. Notably, the carboxylate and sulfate bands related to the asymmetric vibrations of COO^- and -O-SO_3^- removed by 23 cm^{-1} to lower wavenumber values. These results suggest occurrence of hydrogen-bonding between these groups and hydroxyl groups on the surfaces of nanoparticles.

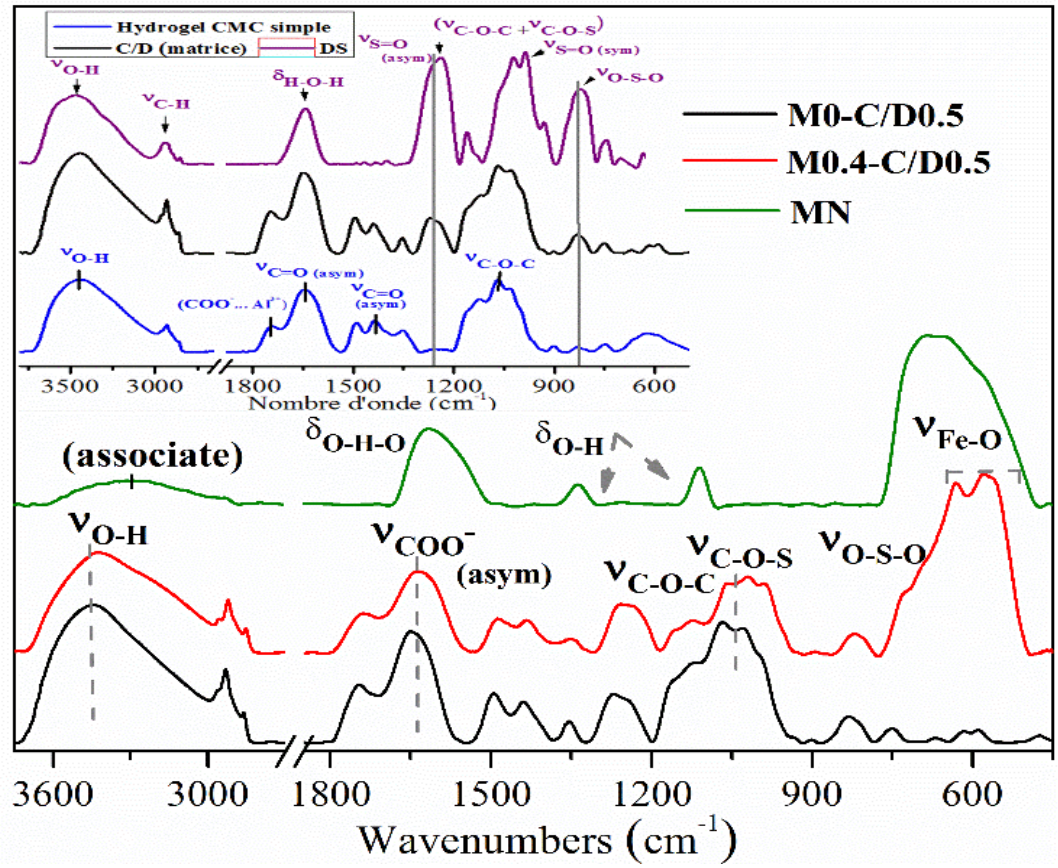

Fig.3. FTIR spectra of free hydrogel, magnetic nanoparticles, and its nanocomposite

The magnetic behavior of the samples was performed at room temperature using VSM analysis at ± 10 kOe and the obtained data are given in Table 1. The saturation magnetization value (SMV) of the nanoparticles MN was 57.73 emu g^{-1}.

Table 1. Magnetic parameters of MN nanoparticles and their nanocomposite beads.

Sample	Ms (emu g^{-1})	Mr (emu g^{-1})	Hc
MN	57.47	0.92	11.79
M**0.4**-y	26.52	0.61	12.58

The magnetic parameters, specifically the remanent magnetization (Mr), are nearly zero for both the magnetic nanoparticles and beads, confirming their superparamagnetic behavior [9]. However, the magnetic beads exhibit lower saturation magnetization values (SMV) compared to the magnetic nanoparticles. This behavior suggests that these values are significantly

influenced by the quantity of nanoparticles encapsulated within the crosslinked hydrogels and the surface effects resulting from the coating of nanoparticles with CMC and DS chains, which themselves have non-magnetic properties. These results suggest that the magnetic beads possess a significant magnetic intensity and can be readily separated from the dye solution using an external magnetic field after adsorption.

TGA analysis was carried out in order to investigate the effect of the nanoparticles on the thermal degradation bihavior of the prepared nanocomposites. TGA/d(TG) thermograms of MN, the matrix and its magnetic nanocomposite were presented in **Fig. 4**.

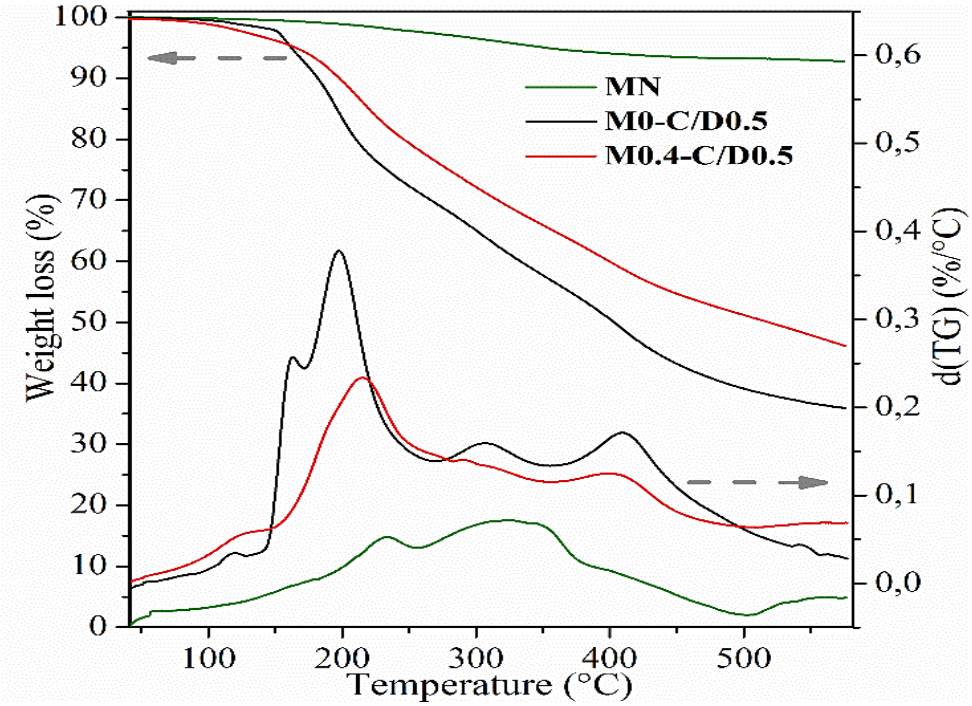

Fig.4. TGA and d(TG) thermograms of Fe_3O_4 nanoparticles, matrix, and its nanocomposite.

The decomposition of MN occurs in two steps, with mass losses of 2.3% at a T_{max} of 230 °C and 3.53% at a T_{max} of 326 °C. These steps correspond to the loss of physisorbed water and dehydroxylation of surfaces, respectively.

The thermal degradation of the magnetic beads follows a similar pattern to that of the matrix, which includes the desorption of physically adsorbed water (first step) and the subsequent removal of structural water, along with depolymerization involving the breaking of C-O and

C-C bonds in the ring units (second and third steps), resulting in the release of volatile products such as CO, CO_2, and H_2O. However, the presence of entrapped nanoparticles within the matrix enhances the thermal stability of the resulting nanocomposite. This enhancement is evident from the increase in T_{max} of the second step, rising from 196 to 214 °C. This improvement is attributed to a barrier effect induced by Fe_3O_4, which, in turn, can increase the cross-linking density through secondary interactions, so limiting the chains mobility [10].

3.2. MB dye adsorption studies

The adsorption data were collected at room temperature while varying different parameters that influence this process. As shown in Fig. 5a, the removal efficiency (R%) exhibits a rapid increase with an increasing adsorbent dose, reaching a maximum at 1 g L^{-1}, reflecting saturation of the adsorption sites [1].

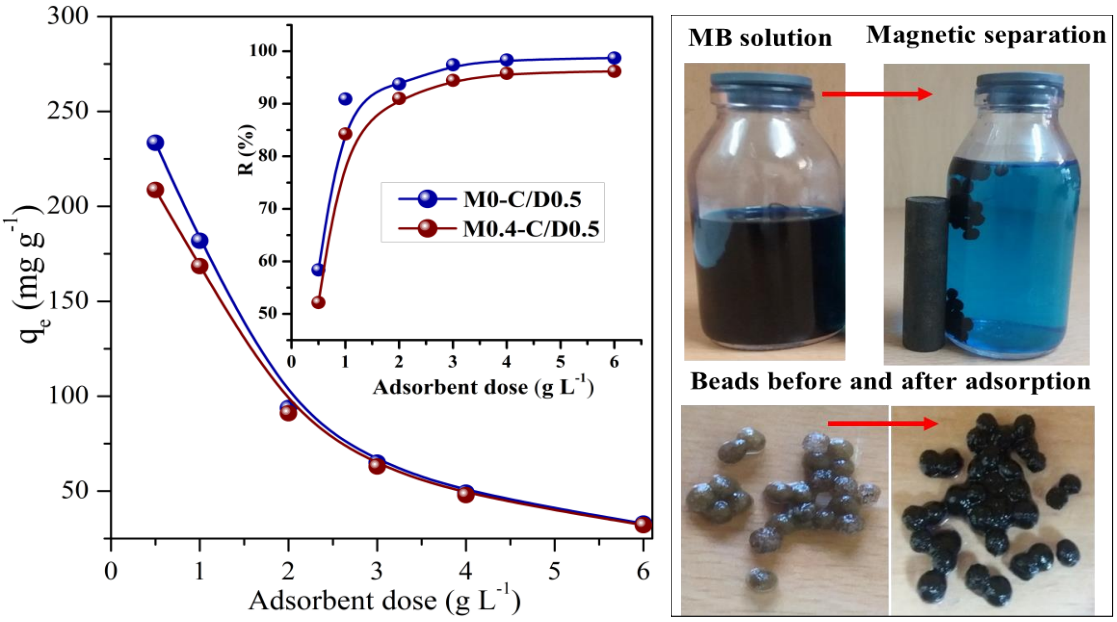

Fig.5. Effect of adsorbent dose on MB adsorption and photographs showing MB solutions and hydrogel beads before and after adsorption and their magnetic separartion.

The kinetic study curves are presented in Fig. 6. It is evident that adsorption follows a three-stage process for all the adsorbents: it initially increases rapidly, then slows down until it reaches a maximum at 6 hours for both the virgin matrix and M0.4-C/D0.5 beads. Beyond this

point, no significant increase is observed. This final step indicates the saturation of the active sites by the dye moleculeThe kinetic pseudo-first order model (Eq. 3) and the pseudo-second order model were applied (Eq. 4) [1-3].

$$q_t = q_{e1}\left(1 - e^{-k_1 t}\right) \qquad (3)$$

$$q_t = \frac{k_2 q_{e2}^2 t}{(1 + q_{e2} k_2 t)} \qquad (4)$$

where, q_e and q_t (mg g^{-1}) denote the amount of adsorbed MB on adsorbents at equilibrium and at time t (min), respectively. k_1 (min^{-1}) and k_2 (g mg^{-1} min^{-1}) refer to the rate constants of pseudo-first-order and pseudo-second-order models, respectively.

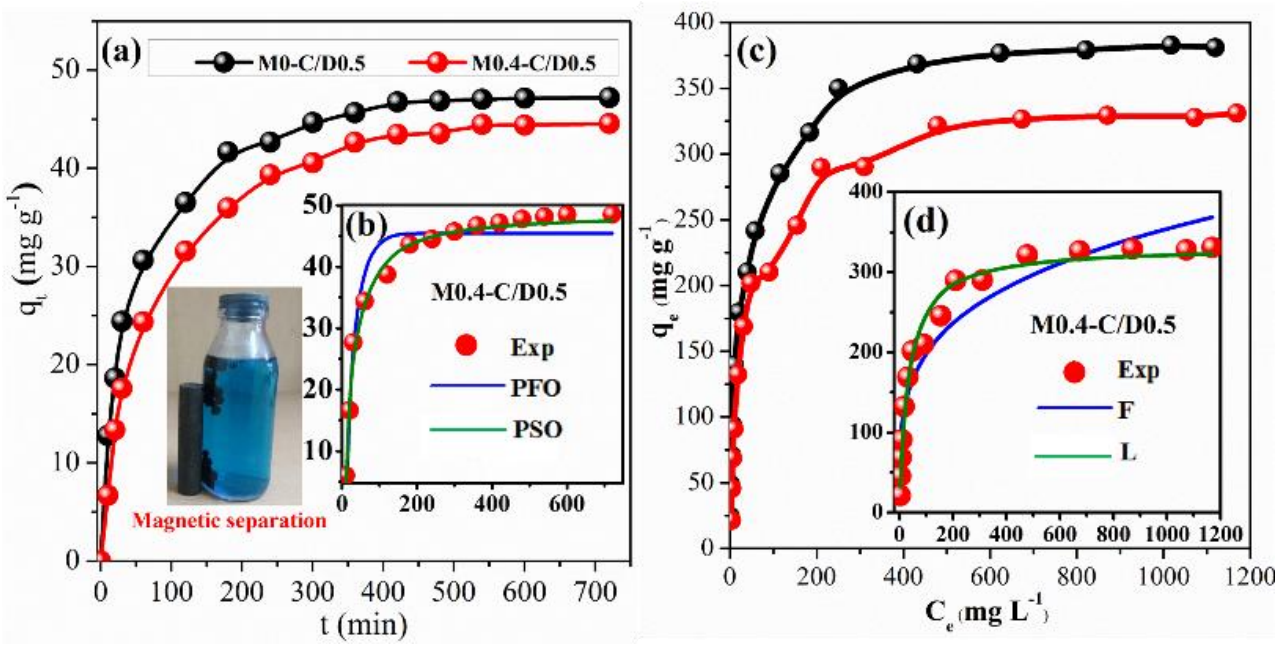

Fig.6. (a, c) Kinetic and isotherm curves (b,d) fitting of experimental data

As observed in Fig. 6b, the qe2 values obtained from the pseudo-second-order plots closely match the experimental data, suggesting that this model is the most appropriate for describing the adsorption of MB on the beads.The effect of varying the initial concentration (C_0) on the

equilibrium adsorption capacity was also examined, and the resulting data are presented in Fig. 6c. Across all adsorbents, an increase in the C_0 of MB leads to a notable increase in the quantity of MB adsorbed until equilibrium is reached. At low concentrations, MB molecules are randomly adsorbed by the active sites on the adsorbents surface. However, at higher C_0, the driving force resulting from the concentration gradient becomes stronger [1], enhancing the adsorption of MB.

The adsorption isotherms were analyzed using the Freundlich (Eq. 5) and Langmuir (Eq. 6) models [1,2], and the corresponding parameters are given in Table 2.

$$q_e = K_F C_e^{1/n} \quad (5)$$

$$q_e = \frac{q_m K_L C_e}{(1 + K_L C_e)} \quad (6)$$

Where, C_e is the equilibrium adsorbate concentration in solution (mg L^{-1}), qe is the amount of adsorbed MB at equilibrium (mg g^{-1}), qm is Langmuir adsorption capacity at equilibrium (mg g^{-1}), K_L is Langmuir adsorption constant (L mg^{-1}). K_F (L g^{-1}) and n are the Freundlich constant and Freundlich distribution factor.

The favorability of the adsorption process can also be expressed using the separation constant RL (Eq. 7). This constant indicates whether the adsorption process is favorable ($0 < R_L < 1$), unfavorable ($R_L > 1$), linear ($R_L = 1$), or irreversible ($R_L = 0$)

$$R_L = \frac{1}{1 + K_L C_0} \quad (7)$$

The results confirm the applicability of the Langmuir model to all adsorbents, indicating a favorable monolayer adsorption process. It's noteworthy that the highest optimal qm value of 380 mg g^{-1} was achieved for the virgin matrix (**M0**-C/D0.5 beads). Additionally, the encapsulation of MN into the network resulted in a slight reduction in its removal capacity

Table 2. Freundlich and Langmuir parameters of isotherm adsorption.

Adsorbent	$q_{e,exp}$ (mg g^{-1})	Freundlich model		
		K_F ($L.g^{-1}$)	n ($g.L^{-1}$)	R^2
M**0**-y	380.91	83.97	4.32	0.969
M**0.4**- y	330.97	63.45	4.01	0.956
Adsorbent	q_m (mg g^{-1})	Langmuir model		
		K_L ($L.g^{-1}$)	R^2	$R_L{}^b$
M**0**-y	380.96	0.04	0.992	0.507
M**0.4**- y	331.82	0.03	0.991	0.563

y= C/D0.5, [b] for C_0 = 25 mg L^{-1}

From Fig 7, the magnetic nanocomposite adsorbents are perfectly regenerated with desorption efficiencies above 94% and then reused without any apparent loss in stability.

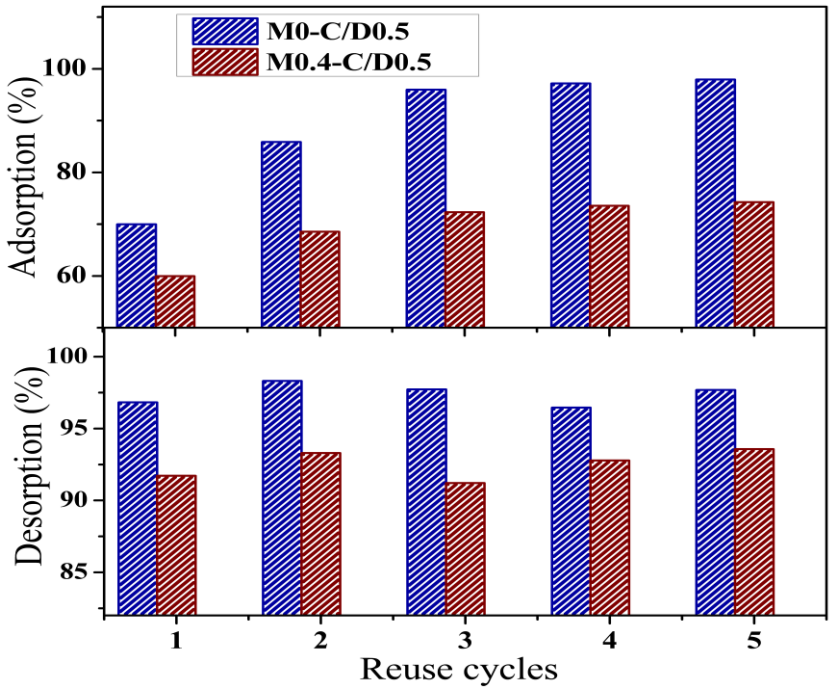

Fig.7. Reuse of milligels in five adsorption/desorption cycles

Compared to their initial state, the regenerated beads exhibit an enhancement in their removal efficiency with each cycle. This phenomenon is directly linked to the residual MB trapped within the beads, which creates additional vacant spaces for further adsorption. However, it's important to note that this improvement is less pronounced for the nanocomposites compared to the matrix. This can be attributed to the relatively simpler and narrower structure of the magnetic beads resulting from the incorporation of MN, which in turn makes the desorption process more challenging.

4. CONCLUSION

Magnetic nanocomposite beads composed of CMC/DS and Fe_3O_4 nanoparticles were synthesized and subjected to comprehensive characterization. These beads were assessed for their effectiveness in adsorbing MB. The kinetics data exhibited conformity with the pseudo-second-order model, while the data fitting to the Langmuir isotherm model confirmed monolayer MB adsorption. Furthermore, the adsorbents displayed remarkable regenerative capabilities, maintaining high performance even after five cycles of reuse.

Thus, our magnetic beads, offering high adsorption capacities and effective magnetic separation properties, are attractive and cost-effective adsorbents for efficiently recovering cationic dyes from contaminated water.

5. REFERENCES

[1] T. Benhalima, H. Ferfera-Harrar, D. Lerari, Optimization of carboxymethyl cellulose hydrogels beads generated by an anionic surfactant micelle templating for cationic dye uptake: Swelling, sorption and reusability studies, Int. J. Biol. Macromol. 105 (2017).

[2] T. Benhalima, H. Ferfera-Harrar, Eco-friendly porous carboxymethyl cellulose/dextran sulfate composite beads as reusable and efficient adsorbents of cationic dye methylene blue, Int. J. Biol. Macromol. 132 (2019).

[3] Ferfera-Harrar, H., Benhalima, T. & Sadi, A. Development of functional chitosan-based superabsorbent hydrogel nanocomposites for adsorptive removal of Basic Red 46 textile dye. Polym. Bull. (2021).

[4] P. Liu, L. Zhang, Adsorption of dyes from aqueous solutions or suspensions with clay nano-adsorbents, Sep. Purif. Technol. 58 (2007) 32–39.

[5] X. Qi, L. Wu, T. Su, J. Zhang, W. Dong, Polysaccharide-based cationic hydrogels for dye adsorption, Colloids Surfaces B Biointerfaces. 170 (2018) 364–372.

[6] W. Tiyaboonchai, J. Woiszwillo, Formulation and characterization of amphotericin Bpolyethyleniminedextran sulfate nanoparticles, J. Pharm. Sci. 90 (2001) 902–914.

[7] G.O. Akalin, M. Pulat, Preparation and characterization of nanoporous sodium carboxymethyl cellulose hydrogel beads, J. Nanomater. 2018 (2018)1-12.

[8] R.A. Ismail, G.M. Sulaiman, S.A. Abdulrahman, T.R. Marzoog, Antibacterial activity of magnetic iron oxide nanoparticles synthesized by laser ablation in liquid, Mater. Sci. Eng. C. 53 (2015) 286–297.

[9] H. Fatima, D.W. Lee, H.J. Yun, K.S. Kim, Shape-controlled synthesis of magnetic Fe_3O_4 nanoparticles with different iron precursors and capping agents, RSC Adv. 8 (2018) 22917–22923.

[10] A. Konwar, A. Gogoi, D. Chowdhury, Magnetic alginate-Fe_3O_4 hydrogel fiber capable of ciprofloxacin hydrochloride adsorption/separation in aqueous solution, RSC Adv. 5 (2015) 81573–81582.